Computational and Structural Biotechnology Journal 18 (2020) 1202–1209

COMPUTATIONAL AND STRUCTURAL BIOTECHNOLOGY JOURNAL

journal homepage: www.elsevier.com/locate/csbj

Desaturase specificity is controlled by the physicochemical properties of a single amino acid residue in the substrate binding tunnel

Aleš Buček [a,b], Mario Vazdar [c], Michal Tupec [a], Aleš Svatoš [a,d], Iva Pichová [a,*]

[a] Institute of Organic Chemistry and Biochemistry of the Czech Academy of Sciences, Flemingovo n., 2, 166 10 Prague 6, Czech Republic
[b] Okinawa Institute of Science and Technology Graduate University, 1919-1 Tancha, 904-0495 Okinawa, Japan
[c] Division of Organic Chemistry and Biochemistry, Ruđer Bošković Institute, Bijenička 54, HR-10000 Zagreb, Croatia
[d] Max Planck Institute for Chemical Ecology, Hans-Knöll-Str. 8, D-07745 Jena, Germany

ARTICLE INFO

Article history:
Received 3 February 2020
Received in revised form 23 April 2020
Accepted 9 May 2020
Available online 14 May 2020

Keywords:
Acyl-CoA desaturase
Manduca sexta
Bombyx mori
Enzymatic specificity
Protein engineering
Molecular dynamics simulations

ABSTRACT

Membrane fatty acyl desaturases (mFAD) are ubiquitous enzymes in eukaryotes. They introduce double bonds into fatty acids (FAs), producing structurally diverse unsaturated FAs which serve as membrane lipid components or precursors of signaling molecules. The mechanisms controlling enzymatic specificity and selectivity of desaturation are, however, poorly understood. We found that the physicochemical properties, particularly side chain volume, of a single amino acid (aa) residue in insect mFADs (Lepidoptera: *Bombyx mori* and *Manduca sexta*) control the desaturation products. Molecular dynamics simulations of systems comprising wild-type or mutant mFADs with fatty acyl-CoA substrates revealed that the single aa substitution likely directs the outcome of the desaturation reaction by modulating the distance between substrate fatty acyl carbon atoms and active center metal ions. These findings, as well as our methodology combining mFAD mutational screening with molecular dynamics simulations, will facilitate prediction of desaturation products and facilitate engineering of mFADs for biotechnological applications.

1. Introduction

Membrane fatty acyl desaturases (mFADs) are present in all eukaryotic organisms and some prokaryotes. They catalyze a highly energetically demanding oxygen-dependent extraction of hydrogen atoms from fatty acyl hydrocarbon chains [1]. Individual members of the mFAD gene family exhibit rather narrow substrate specificity with respect to the fatty acyl head group, chain length, and pre-existing double bonds. mFAD homologs also show distinct regio- and stereospecificities with respect to the position and configuration of the double bond(s) they introduce, respectively [2,3]. The vast repertoire of mFAD specificities results in an immense number of unsaturated fatty acyls (UFAs) with diverse physical and chemical properties that underlie their biological roles as cell membrane lipid components or precursors of signaling molecules including prostaglandins, leukotrienes, and insect pheromones [2–4].

Despite the fundamental role of mFADs in determining the composition of UFA pools within organisms, the structural determinants of mFAD specificities remain poorly understood, chiefly due to the difficulties of experimentally determining membrane protein structures. Two recent breakthrough structures of mammalian mFADs indicate that the acyl chain of the substrate is enclosed in a sharply kinked hydrophobic binding tunnel, which presumably constrains the substrate chain length and position with respect to the mFAD active center. This substrate binding tunnel likely provides a basis for the specificity of the desaturation reaction. The active center, which activates molecular oxygen necessary for the desaturation reaction, is formed by a di-iron cluster coordinated by His residues [5,6].

To uncover the structural and sequential motifs that govern the outcome of desaturation reactions, more than a hundred mFAD genes and mutants have been cloned and functionally characterized in a yeast expression system [5,7–20]. These studies identified an extensive collection of mFAD mutations that influence mFAD specificity, yet insights into universal mechanisms of desaturation specificity remain limited. Ideally, a search for mFAD specificity determinants would 1) use an experimentally determined mFAD structure [5] or homology-based model [13,15–17], 2) cross-validate the effect of the identified mutations in more distantly related mFADs, and 3) systematically screen the effect of a range

* Corresponding author.
E-mail address: iva.pichova@uochb.cas.cz (I. Pichová).

https://doi.org/10.1016/j.csbj.2020.05.011

of amino acid (aa) residues at the candidate specificity-determining aa sites. Such a systematic approach has not yet been applied to study mFAD structure–function relationships.

Homology-based modeling of mFADs using either of the two available mFAD structures [5,6] represents a feasible and increasingly accurate alternative to experimental structure determination [21,22]. Previously, mapping aa residues and regions critical for mFAD specificity onto mFAD structural models localized the specificity-determining regions to the vicinity of the substrate-binding channel opening [15], distal end of the substrate-binding channel [5,13], kink of the substrate-binding channel [17], and vicinity of the iron atoms in the active center [15,16].

To shed light on the mechanisms of specificity determination in mFADs, we used as a model system two pheromone-producing mFADs, *Msex*D2 and *Msex*D3, from the tobacco hornworm moth *Manduca sexta*. This pair of mFADs with high sequence similarity exhibits distinct desaturase selectivities and specificities with C14 and C16 fatty acyl-CoA substrate resulting in production of a spectrum of mono-, di- and tri-unsaturated fatty acyls (Fig. 1) [17]. Notably, reciprocal swapping of amino acid residue Ala224/Ile224 within the predicted substrate-binding tunnel leads to exchange of the desaturase specificities and selectivities of *Msex*D2 and *Msex*D3 [17]. However, the mechanism by which a single amino acid residue modulates the desaturase substrate preference and the position of introduced double bond(s) remains elusive. Here we combine 1) experimental characterization of mFAD mutants constructed by systematic replacement of a single aa position with a panel of residues, 2) assessment of the mutation effect in a more distantly related mFAD from the silkworm moth *Bombyx mori*, and 3) molecular dynamics (MD) simulations of homology-based mFAD-substrate complexes. Our results provide mechanistic insights into how steric and hydrophobic effects of aa residues in the mFAD substrate-binding channel influence the position of the substrate with respect to the active center and thus govern the outcome of the desaturation reaction.

2. Materials and methods

2.1. Desaturase cloning and site-directed mutagenesis

The empty expression plasmid was provided by Holz et al. [23]. The pYEXTHS-BN expression plasmids bearing *Msex*D2, *Msex*D3, *Msex*D2-Ile224, and *Msex*D3-Ala224 coding regions with N-terminal His6tags under the control of the Cu^{+2}-inducible promoter *CUP1* were previously constructed in our laboratory [17]. Coding regions of wt *B. mori* desaturase *Bmor*D1 [24] and its single-aa mutant *Bmor*D1-Ile227 were optimized for yeast codon usage, custom synthesized (GenScript), and subcloned into the pYEXTHS-BN vector using the primers BmorD1(opt)_BamHI_F and BmorD1(opt)_EcoRI_R (Table S1). The corresponding GenBank accession numbers are MG450705 and MG450706. Plasmids bearing single point mutations coding for Gly224, Thr224, Val224, and Phe224 were constructed by site-directed mutagenesis with Phusion HF DNA polymerase (New England BioLabs) and mutagenesis primers (for primer list, see Table S1) to introduce single point mutations into pYEXTHS-BN vectors bearing either the *Msex*D2 or *Msex*D3 ORF. The cycling conditions comprised initial denaturation at 98 °C (2 min); 30 amplification cycles consisting of the following steps: 98 °C (10 s), 58 °C (20 s) and 72 °C (6 min); and a final extension step at 72 °C for 10 min. The PCR reaction product was treated with *Dpn*I endonuclease for 1 h at 37 °C, and 1 μl of the reaction mixture was transformed into competent *E. coli*. All vectors were verified by sequencing.

2.2. Functional expression in yeast

The pYEXTHS-BN constructs and an empty pYEXTHS-BN vector (control) were transformed into a desaturase- and elongase-deficient double mutant *Saccharomyces cerevisiae* strain (MAT**a** *elo1:HIS3 ole1:LEU2 ade2 his3 leu2 ura3;* further referred to as *elo*1-Δ*ole*1Δ) [25] using the S.c. EasyComp Transformation Kit (Invitrogen) according to the manufacturer's instructions. Transformed colonies were selected on agar plates with synthetic complete media lacking uracil [SC-U: 0.67% yeast nitrogen base without amino acids, 2% glucose, 2% agarose, supplemented with Brent supplement mix without uracil (ForMedium), according to the manufacturer's instructions] supplemented with a mixture of unsaturated fatty acids [palmitoleic and oleic acid, each 0.05 mM, solubilized by 0.25% tergitol (type NP-40, Sigma-Aldrich)] to maintain the growth of the *Z*9-UFA deficient *elo*1Δ*ole*1Δ yeast strain.

Yeast strains were cultivated in 20 ml liquid SC-U medium supplemented with palmitoleic and oleic acid (each 0.05 mM), 0.25% tergitol, and 0.5 mM $CuSO_4$ to induce heterologous expression of mFADs under the control of CUP1 promoter. Where indicated,

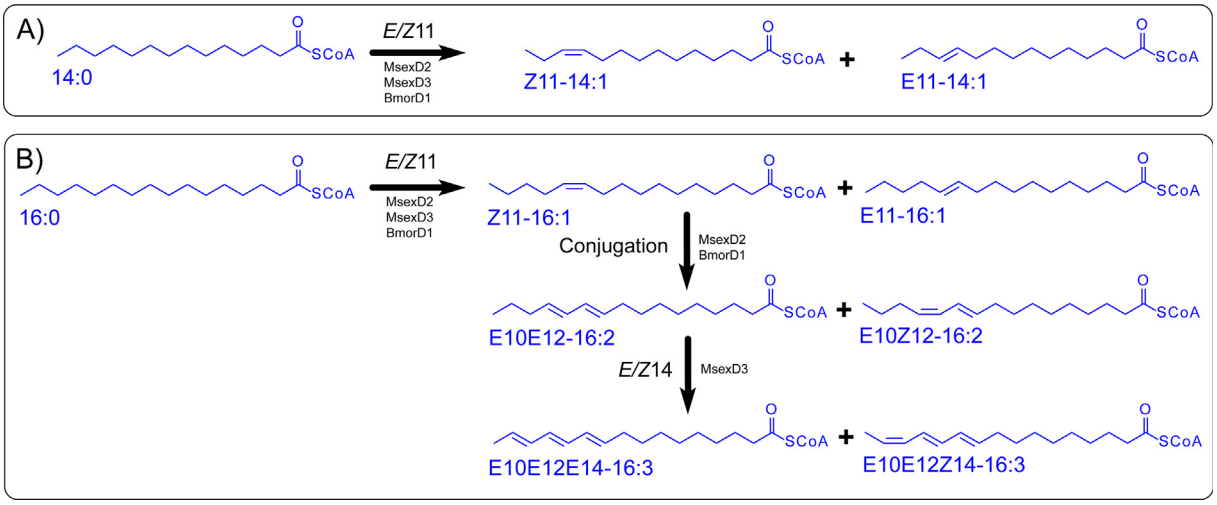

Fig. 1. Overview of desaturation reactions catalyzed by *M. sexta* and *B. mori* wild-type mFADs. The products of desaturation of tetradecanoyl-CoA (**A**) and hexadecanoyl-CoA (**B**) substrates via wild-type mFADs from *M. sexta* and *B. mori* as determined in yeast expression system. The position of introduced double bonds and the enzymes catalyzing these steps are shown along the reaction arrows. Conjugation step refers to synthesis of conjugated double bond system from monounsaturated precursor via 1,4-dehydrogenation which is formally accompanied by substrate double bond rearrangement [51]. Based on references [17,24] and this study.

yeast strains were cultivated with methyl *Z*11-hexadecenoate (*Z*11-16:1) supplemented in the induction medium to a final concentration of 0.1 mM or methyl *E*10*E*12-hexadecadienoate (*E*10*E*12-16:2) supplemented to a final concentration of 0.25 mM. Fatty acids 14:0 and 16:0, which served as substrates for mFAD *E*/*Z*11-desaturase activities, were naturally abundant in yeast cells and were not supplemented into the cultivation media, with the exception of cultivations of *Bmor*D1-transformed yeast cultures for analysis of C14 products, which were supplemented with 0.25 mM methyl tetradecanoate. The yeast liquid cultures were cultivated for 3 days until they reached the stationary phase and the yeast cell biomass was harvested by centrifugation as previously described [26]. Heterologous mFAD expression was monitored by western blotting with anti-His6tag antibody [27]. All mFADs migrated on SDS-PAGE as apparently lower molecular weight proteins compared to their calculated protein molecular weights of 37.2 kDa and 39.6 kDa, respectively, presumably due to anomalous migration of transmembrane proteins [28]. Total cellular lipids were transesterified to fatty acid methyl esters (FAMEs) and extracted as described by Matoušková *et al.* [29].

2.3. GC/MS analysis

Conditions for GC/MS analysis of extracts from yeasts expressing MsexD2 and MsexD3 variants, and from yeasts expressing BmorD1 supplemented with methyl tetradecanoate were as follows: carrier gas, He, 1 ml/min; splitless injection, 1 µl; injector temperature, 220 °C; thermal gradient, 40 °C for 2 min, 40 °C to 140 °C at 70 °C/min, 140 °C to 240 °C at 3 °C/min, 240 °C to 280 °C at 20 °C/min, and 280 °C for 5 min. The temperature program was terminated at 230 °C and held for 15 min when the DB-WAX column was used. The extracts from yeasts expressing BmorD1 (except for those from methyl tetradecanoate supplementation) were analyzed as follows: carrier gas, He, 1 ml/min; 1 µl split injection 5:1; injector temperature, 250 °C; DB–5 ms column; thermal gradient, 140 °C for 1 min, 140 °C to 230 °C at 3 °C/min, 230 °C to 320 °C at 20 °C/min, and 320 °C for 3 min.

The relative FAME quantity of a particular FAME was calculated as the total ion current (TIC) area of its peak divided by the sum of TIC areas of all major FAME peaks in the chromatogram; the resulting value was then multiplied by 100%. The differences between mean values of relative FAME production at a significance level of 0.05 were calculated using ANOVA with a "post-hoc" Tukey's test using R language and agricolae v1.2–6 R-package [30].

2.4. Desaturase sequence analysis

Desaturase sequences retrieved from NCBI GenBank were aligned using the Muscle algorithm [31] and formatted using JalView [32].

2.5. Structure modeling, molecular dynamics simulations and quantum-chemical calculations

The initial structures of wt *Msex*D2 and *Msex*D3 were generated using the homology modeling module in YASARA [21], with default parameters and charges corresponding to pH 7 and using the structure of mammalian mFAD with PDB ID code 4YMK as a template [5,17]. Wt *Msex*D2, corresponding mutants, and ions were described with the Amber99SB force field [33], while parameters for fatty acyl-CoA substrates were based on the Slipids force field [34–36]. All missing bonding and nonbonding parameters of fatty acyl-CoA substrates in the existing Slipids force field were updated with compatible CHARMM36 parameters, while atomic charges were calculated by the Merz-Singh-Kollman scheme [37] consisting of B3LYP/6-31G(d) geometry optimization and a subsequent single point ESP charge calculation using the B3LYP/cc-pVTZ method. All systems were solvated in a cubic box of dimensions 10.0 nm × 10.0 nm × 10.0 nm with approximately 31,500 TIP3p water molecules [38]. The total charge of the *Msex*D2 protein was +9, whereas the charge of the fatty acyl-CoA substrates was −4. Electroneutrality of the system was maintained by adding 5 chloride counterions. Two zinc atoms in the *Msex*D2 protein were constrained using umbrella potential with a force constant of 1000 kJ mol^{-1} nm^{-2} to keep the active site of the protein stable. Zn atoms were not covalently bound to histidine residues and were allowed to freely accommodate in the active site. The stability of the active site was checked by monitoring its hydration and water coordination around histidines, which was kept roughly constant throughout MD simulations. At this stage, simulations with *Msex*D3 were unstable for most mutants and the substrate was not optimally fitted in the active site, and therefore further MD simulations were performed with the focus on wt *Msex*D2 and five *Msex*D2 mutants with single aa substitutions at position 224 (Thr224, Val224, Ile224, Gly224 and Phe224) together with two different fatty acyl-CoA substrates, 16:0 and *E*10*E*12-16:2.

All MD simulations were run for 100 ns after initial equilibration of at least 10 ns with employed periodic boundary conditions in three dimensions. Long range electrostatic interactions beyond the non-bonded cutoff of 1.0 nm were described with the particle-mesh Ewald procedure [39] using Fourier spacing of 0.12 nm. The real space Coulomb interactions were cut off at 1.0 nm and van der Waals interactions were cut off at 1.4 nm. Pressure of 1 bar was maintained using the Parrinello–Rahman algorithm [40] with a coupling constant of 10 ps^{-1}. The temperature of 310 K was controlled with the Nose–Hoover thermostat with a coupling constant of 0.5 ps^{-1} [41] independently for the protein with the fatty acyl substrate and water sub-systems. All bonds within protein and the fatty acyl-CoA substrate were constrained using the LINCS algorithm [42]. O–H bonds in water were kept constant using the SETTLE method [43]. Equations of motion were integrated using the leap-frog algorithm with a time step of 2 fs. All MD simulations were performed using the GROMACS program package, version 4.5.4 [44]. The number of molecular contacts between substrate carbon atoms and two Zn atoms in the active site below 0.7 nm, average distances, time evolution of distances, and standard deviations of average distances (substrate dynamics) were calculated for the duration of the MD simulations.

3. Results and discussion

3.1. aa224 in MsexD2 and MsexD3 fine tunes the desaturase activities and specificities

Our previous research highlighted aa224 residue as critical determinant of mFAD specificity in *Msex*D2 and *Msex*D3 by showing that reciprocal exchange of Ala224 and Ile224 residues which are present in the wild-type (wt) *Msex*D2 and *Msex*D3, respectively, leads to exchange of their desaturase specificities [17]. To uncover the mechanistic details of the specificity switch, here we first constructed a set of *Msex*D2 and *Msex*D3 mutants with glycine, alanine, valine, isoleucine, phenylalanine, or threonine at position 224 and expressed them in a yeast expression system. Western blotting of yeast lysates showed generally higher expression levels of *Msex*D3 and its mutants than that of *Msex*D2 and its mutants (Fig. 2). The expression levels among all wt and mutant *Msex*D2 and *Msex*D3, respectively, were comparable (Fig. 2), indicating that the aa224 mutations did not systematically or substantially influence mFAD protein levels in yeast cells. The relative production of UFAs by heterologously expressed mFADs was quantified by GC/MS analyses of fatty acyl methyl esters (FAMEs) transesterified

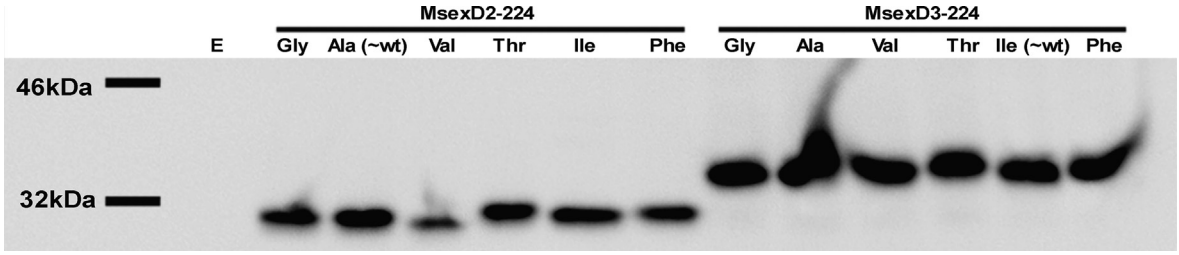

Fig. 2. Detection of heterologously expressed mFADs in yeast lysates by western blotting with anti-His6tag antibody. Yeast lysates from 50 μl of yeast culture were loaded in each lane. Anti-His6tag antibody was used to visualize the His-tagged mFADs. The bars on the left indicate positions of protein standard bands of 32 and 46 kDa. The lysate of a yeast strain transformed with an empty expression vector is marked "E."

from yeast total cellular lipids. The relative FAME quantities were then used to compare the approximate mFAD activity levels of the individual mutants and wt.

Mutations at aa224 in *Msex*D2 and *Msex*D3 led to a range of effects, including gain of novel or loss of original desaturase specificities, as well as increases or decreases in desaturase activity relative to the wt mFADs (Fig. 3). Desaturase activity was generally higher in *Msex*D3 and its mutants, probably as a result of their higher expression levels (Fig. 2). *Msex*D2- and *Msex*D3-aa224 mutants exhibited strikingly similar trends in desaturase specificity and activity with respect to the aa224 side chain volume (Fig. 3), leading us to interpret the changes in mFAD enzymatic specificities in terms of the steric effect of the aa224 side chain. However, other physicochemical properties of the aa224 side chain, such as its hydrophobicity, also are likely to contribute to the observed shifts in UFA products.

For *Msex*D2, *Msex*D3, and their mutants, *Z*11-desaturation of the C16 substrate and conjugation activity (i.e., production of conjugated *E*10*E*/*Z*12-16:2 by a combination of desaturation and shift in preexisting double bond position) followed the same trend and were favored by less bulky Ala224 and Thr224 residues (Fig. 3D,E). In contrast, bulkier Val224 and Ile224 favored *E*/*Z*14-desaturase activity with the *E*10*E*12-16:2 substrate. The least bulky and the bulkiest aa224 residues, Gly and Phe, respectively, resulted in an overall decrease in or loss of desaturase activity (Fig. 3C).

Z/*E*11-desaturation of a short substrate (C14) in both *Msex*D2, *Msex*D3, and their mutants was favored by bulkier aa224 residues (Fig. 3A, B). In contrast to desaturation of the C16 substrate, *Z*/*E*11 desaturation of the C14 substrate did not dramatically decrease for the bulkiest Phe residue. These results suggest that steric constraints for desaturation of shorter fatty acyl substrates, such as C14, might be relaxed compared to fatty acyl substrates with longer chains.

3.2. The role of aa224 as a desaturase specificity switch is conserved in B. mori mFAD

To evaluate whether the role of aa224 in determining desaturase specificity also is conserved in other mFADs, we mutated *Bmor*D1, a pheromone-producing mFAD from the silk moth *Bombyx mori* [24], which shares 62.9% and 60.2% sequence identity with *Msex*D2 and *Msex*D3, respectively (Fig. S1). *Bmor*D1 desaturase specificity closely parallels that of *Msex*D2 by exhibiting both *Z*11-desaturase and conjugase activity [24]. Despite these similarities, the gene tree of mFAD gene family does not support one-to-one orthology between *Msex*D2 and *Bmor*D1 [17]. Instead, it is plausible that the conjugase activities of *Msex*D2 and *Bmor*D1 evolved independently and convergently.

Thr227 in *Bmor*D1 is homologous to Ala224 in *Msex*D2 and Ile224 in *Msex*D3 (Fig. S1). Replacing this residue with Ile significantly decreased production of *Z*11-16:1 compared to wt *Bmor*D1 and abolished production of *E*10*E*12-16:2 and *E*10*Z*12-16:2 (Fig. 3-C-E). Remarkably, this mutation also conferred novel *E*/*Z*14-desaturase activity onto the *Bmor*D1-Ile227 mutant (Fig. 3F, G). The *Bmor*D1-Ile227 mutant thus acquired a desaturase specificity profile close to that of *Msex*D2-Ile224 and *Msex*D3-Ile224 (wt). These results indicate that mFAD specificity is to a large extent controlled by conserved mechanisms and can be tuned by changes as subtle as a single aa substitution in the kink of the FA-binding tunnel. The presence of Ile224 alone, however, is apparently not sufficient to install *E*/*Z*14-desaturase specificity across all lepidopteran mFADs, as several moth mFADs with Ile at the position homologous to aa224 do not exhibit *E*/*Z*14-desaturase specificity (Fig. S2) [45–49]. In these mFADs, structural changes in other regions likely further modulate the desaturase specificity.

3.3. Mutations of aa224 modulate the intermolecular distances between substrate and active center

To uncover the mechanistic details of the experimentally observed desaturase specificity switch**,** we performed MD simulations of complexes of mFADs with fatty acyl substrates. We analyzed the approach of a reactive fatty acyl substrate bond to the mFAD active site metal ions and overall substrate dynamics (quantified as standard deviation of average distances between substrate carbon atoms and Zn atoms in the active site).

First, we generated homology models of *Msex*D2 and *Msex*D3 with substrates 16:0 and *E*10*E*12-16:2 inserted in the substrate binding tunnel, using mammalian mFAD structure as a template [5,17]. Our models included active center Zn ions rather than the *in vivo* catalytically active iron ions [1] to comply with the experimentally determined mammalian mFAD structures [5,6]. In the *Msex*D2 models, the C11-C12 atoms of 16:0 and the C14-C15 atoms of *E*10*E*12-16:2, where desaturation occurs, are positioned in the vicinity of two active center Zn ions. The fatty acyl chain is deeply inserted into the substrate binding tunnel and wrapped around the kink in the tunnel formed by aa224 (Fig. 4A, E). We performed MD simulations with both *Msex*D2 and *Msex*D3. However, the MD simulations of *Msex*D3 were unstable and we therefore proceeded with simulations of *Msex*D2 and its mutants. Since the panel of amino acid residues introduced at position aa224 had comparable effect on desaturase specificity in both *Msex*D2 and *Msex*D3 backgrounds, we assume that either of *Msex*D2 and *Msex*D3 are suitable for simulations of the desaturase specificity switch. Nevertheless, the instability of *Msex*D3 in MD simulations is surprising, given the high overall sequence identity of *Msex*D3 and *Msex*D2 [91% in the homologous 321-aa region (Fig. S1)]. The instability of *Msex*D3 model in MD simulations could be explained by increased constrain of the substrate imposed by bulkier Thr223 in *Msex*D3 (as compared to Ala223 in *Msex*D2). Assuming certain level of force field inaccuracy in the MD simulations, Thr223 could excessively

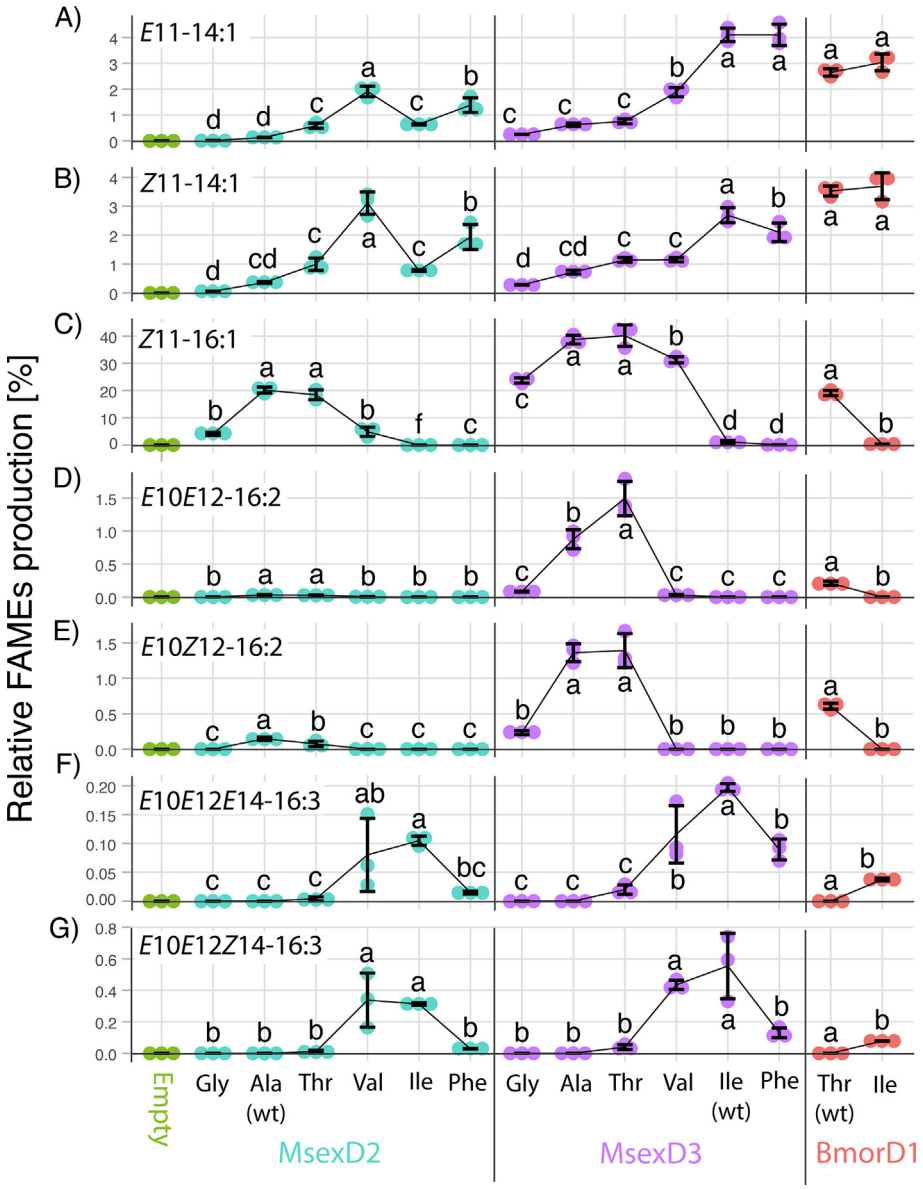

Fig. 3. Production of unsaturated fatty acids by wild-type and mutant *Msex*D2, *Msex*D3, and *Bmor*D1 desaturases. Relative abundances of monounsaturated UFAs *E*11-14:1 (A), *Z*11-14:1 (B), and *Z*11-16:1 (C); di-unsaturated UFAs *E*10*E*12-16:2 (D) and *E*10*Z*12-16:2 (E); and tri-unsaturated UFAs *E*10*E*12*E*14-16:3 (F) and *E*10*E*12*Z*14-16:3 (G) in lipid extracts of yeast strains heterologously expressing mFADs. The amino acid residues are listed in order of their increasing mean volume, as adopted from Harpaz *et al.* [50]. "Empty" represents the yeast strain transformed with an empty expression plasmid. The relative fatty acyl abundances values are the average of three yeast cultivation experiments ± SD, and the colored points indicate individual data points. The mean values which are significantly different (alpha = 0.05) in ANOVA with "post-hoc" Tukey's test are marked with different letters.

constrain the substrate in the MD models and render the complex unstable. We have previously demonstrated that replacement of Ala223 by Thr223 in *Msex*D2 decreases its overall desaturase activity [17] which supports the possible role of Thr223 as a constraint in substrate binding.

3.3.1. MD simulations of MsexD2 with 16:0 substrate

Calculations indicated that *Msex*D2-Thr224 and wt *Msex*D2 (Ala at position 224) with the 16:0 substrate exhibits the shortest average distances between the active site Zn atoms of mFAD and the carbon atoms of the C11-C12 single bond, as well as the largest total number of contacts (Table S2, Fig. 4B,C). These *Msex*D2 variants also exhibited the highest *Z*11-desaturase activity toward the 16:0 substrate among the experimentally characterized mFADs (Fig. 3C). The next shortest average Zn/C11-C12 distances and numbers of Zn/C11-C12 contacts were calculated for *Msex*D2–Ile224 and *Msex*D2-Val224 (Fig. 4B,C). Notably, MD simulation statistics of *Msex*D2–Ile224 with 16:0 substrate are suggesting higher desaturase activity than detected in experiments. This disagreement could be caused by our inability to fully describe the desaturase specificity mechanism in terms of simple MD simulation statistics. In *Msex*D2-Gly224, the average distance between the active site and substrate carbon atoms was large (greater than 1 nm), in agreement with the lower *Z*11-desaturase activity of this mutant. The large average Zn/C11-C12 distances calculated for the *Msex*D2-Phe224 complex with 16:0 suggest that the bulky, hydrophobic Phe side chain hinders the approach of C11-C12 atoms to the active center (Table S2, Fig. 4C), explaining the loss of desaturation activity (Fig. 3C).

In summary, the numbers of contacts and average distances between the C11-C12 atoms of the 16:0 substrate and the Zn active center ions are in generally good agreement with the

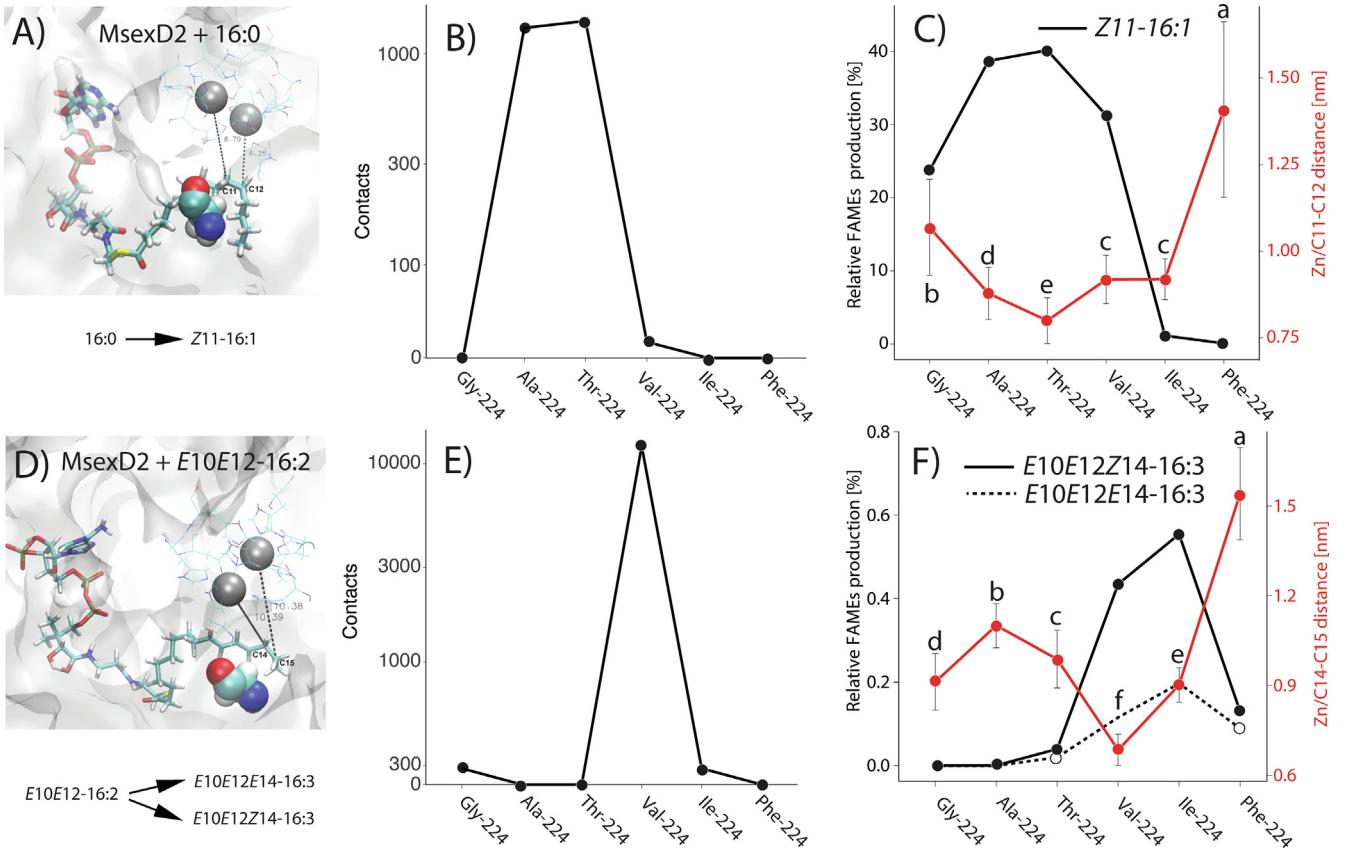

Fig. 4. Molecular dynamics simulations of *Msex*D2 with 16:0-CoA (A, B, C) and *E*10*E*12-16:2-CoA (D, E, F) substrates in the substrate-binding tunnel. Snapshots from MD simulations of *Msex*D2 with 16:0-CoA (A) and *E*10*E*12-16:2-CoA (D) substrates show Ala224 in van der Waals representation; Zn atoms in the active site are shown in grey surrounded by His residues and water molecules. Atoms belonging to the single bond of the substrate where desaturation takes place are labeled, along with the corresponding distance to Zn atoms in the active site. The total number of contacts (less than 0.7 nm) between the Zn atoms in the enzyme active center and the C11-C12 atoms of 16:0-CoA (B) and the C14-C15 atoms of *E*10*E*12-16:2-CoA (E) are indicated. The average distances ± SD between Zn atoms and desaturated carbon atoms are plotted together with relative unsaturated fatty acyl production (C,F) reproduced from Fig. 3, with SD bars omitted for clarity. The average distances which are significantly different (alpha = 0.05) in ANOVA with "post-hoc" Tukey's test are marked with different letters.

experimentally determined *Z*11-desaturase activity of wt *Msex*D2 and its mutants. We observed disagreement of MD simulation and experiments for *Msex*D2–Ile224 with 16:0 substrate which however does not invalidate our ability to identify optimal aa224 residues for *Z*11-desaturase activity using MD simulation statistics.

3.3.2. MD simulations of MsexD2 with 16:2 substrate

In MD simulations of wt and mutant *Msex*D2 with the *E*10*E*12-16:2 substrate, *Msex*D2-Val224 exhibited the shortest distance and the highest number of intermolecular contacts between the C14-C15 atoms of *E*10*E*12-16:2 and the Zn ions (Fig. 4E, F). These MD parameters are in agreement with the experimental finding that *Msex*D2-Val224 has the highest *E*/*Z*14-desaturase activity of the mFADs characterized. The next shortest distance between C14-C15 and Zn ions was observed for *Msex*D2-Ile224, which also gained *E*/*Z*14-desaturase specificity (Fig. 3F,G). *Msex*D2-Ala224 and *Msex*D2-Phe224 exhibited very large distances and no contacts between C14-C15 and Zn, in good agreement with the absence and very low *E*/*Z*14-desaturase activity observed for wt *Msex*D2 and *Msex*D2-Phe224, respectively (Table S2, Fig. 3F,G and Fig. 4E F). The relatively close approach of the C14-C15 substrate bond to the Zn ions and higher substrate dynamics (Table S3, Fig. S4C) may explain retention of low *E*/*Z*14-desaturase activity in *Msex*D2-Thr224 (Fig. 3F,G). *Msex*D2-Gly224 with the *E*10*E*12-16:2 substrate exhibited an intermediate average distance and similar number of C14-C15-Zn contacts as *Msex*D2-Ile224 (Fig. 3E,F and Fig. S4A, C, Table S3) but did not exhibit any detectable *E*/*Z*14-desaturase activity (Fig. 3F,G). Quantitative disagreement of MD simulations and experiments for *Msex*D2-Gly224 with *E*10*E*12-16:2 substrate however does not interfere with our ability to predict Val224 and Ile224, respectively, as optimal residues for *E*/*Z*14-desaturation of *E*10*E*12-16:2 substrate.

Together, the MD simulations revealed that the average distances between the active center metal ions and the substrate carbon atoms at which desaturation is predicted to occur, along with the number of contacts and substrate dynamics, are remarkably good predictors of mFAD specificities. Our experiments and MD simulations can be interpreted in terms of steric effects, as we identified distinct optimal aa224 side chain volumes for *Z*11-desaturase activity with the 16:0 substrate and *E*/*Z*14-desaturase activity with *E*10*E*12-16:2. For desaturation of the 16:0 substrate, the optimal aa224 side chain volume was 26–56 Å^3 (Ala-Thr), while for the *E*10*E*12-16:2 substrate, the optimum was shifted towards more bulky Val and Ile residues with side chain volume ~ 75–101 Å^3 (see Harpaz et al. for amino acid side chain volume calculations [50]). The approach of substrate carbon atoms to the mFAD active center ions is likely also modulated by hydrophobic effects of the aa224 side chain. The aa224 residues that bring substrate most closely to the active center metal ions through steric and hydrophobic interactions exhibit the highest desaturase activity. Future studies using additional mFADs and expanded panels of amino acid residues will likely further refine the relative contributions of hydrophobic and steric effects to the approach of substrate carbon atoms to the active center.

4. Conclusion

In summary, we show that a combination of 1) candidate mutation screening with a panel of amino acid residues, 2) cross-validation of the mutation effect in distantly sequentially related mFADs, and 3) molecular dynamics simulations has the potential to uncover mechanistic details of desaturation specificity. Our results indicate that the side chain volume of a single amino acid residue in the mFAD binding tunnel controls the approach of substrate carbon atoms to the active center metal ions. This single residue thus directs the outcome of the mFAD-catalyzed desaturation. Our approach could help compensate for the scarcity of experimentally determined mFAD protein structures by predicting desaturase reaction outcomes from the mFAD protein sequence and ultimately enabling engineering of mFADs with desired enzymatic properties for biotechnological applications.

Declaration of Competing Interest

The authors declare that they have no known competing financial interests or personal relationships that could have appeared to influence the work reported in this paper.

Acknowledgements

This work was financially supported by the project “ChemBioDrug” CZ.02.1.01/0.0/16_019/000729 from the Ministry of Education of the Czech Republic and project RVO 61388963 from the Academy of Sciences of the Czech Republic.

Author contributions

IP and AB conceived the study. AB, MV, AS, IP participated in research design. AB, MV, MT performed the experiments. All authors analyzed the data. AB, MV, MT, IP wrote the original draft of the manuscript and all authors approved the final version.

Appendix A. Supplementary data

Supplementary data to this article can be found online at https://doi.org/10.1016/j.csbj.2020.05.011.

References

[1] Behrouzian B, Buist PH. Fatty acid desaturation: variations on an oxidative theme. Curr Opin Chem Biol 2002;6:577–82.
[2] Shanklin J, Guy JE, Mishra G, Lindqvist Y. Desaturases: emerging models for understanding functional diversification of diiron-containing enzymes. J Biol Chem 2009;284:18559–63. https://doi.org/10.1074/jbc.R900009200.
[3] Sperling P, Ternes P, Zank TK, Heinz E. The evolution of desaturases. Prostaglandins Leukot Essent Fatty Acids 2003;68:73–95.
[4] Tupec M, Buček A, Valterová I, Pichová I. Biotechnological potential of insect fatty acid-modifying enzymes. Zeitschrift Für Naturforsch C 2017;72:387–403. https://doi.org/10.1515/znc-2017-0031.
[5] Bai Y, McCoy JG, Levin EJ, Sobrado P, Rajashankar KR, Fox BG, et al. X-ray structure of a mammalian stearoyl-CoA desaturase. Nature 2015;524:252–6. https://doi.org/10.1038/nature14549.
[6] Wang H, Klein MG, Zou H, Lane W, Snell G, Levin I, et al. Crystal structure of human stearoyl–coenzyme A desaturase in complex with substrate. Nat Struct Mol Biol 2015;22:581–5. https://doi.org/10.1038/nsmb.3049.
[7] Meesapyodsuk D, Qiu X. Structure determinants for the substrate specificity of acyl-CoA Δ9 desaturases from a marine copepod. ACS Chem Biol 2014;9:922–34. https://doi.org/10.1021/cb400675d.
[8] Gagné SJ, Reed DW, Gray GR, Covello PS. Structural control of chemoselectivity, stereoselectivity, and substrate specificity in membrane-bound fatty acid acetylenases and desaturases. Biochemistry 2009;48:12298–304. https://doi.org/10.1021/bi901605d.
[9] Rawat R, Yu XH, Sweet M, Shanklin J. Conjugated fatty acid synthesis: Residues 111 and 115 influence product partitioning of *Momordica charantia* conjugase. J Biol Chem 2012;287:16230–7. https://doi.org/10.1074/jbc.M111.325316.
[10] Broadwater Ja, Whittle E, Shanklin J. Desaturation and hydroxylation. Residues 148 and 324 of *Arabidopsis* FAD2, in addition to substrate chain length, exert a major influence in partitioning of catalytic specificity. J Biol Chem 2002;277:15613–20. https://doi.org/10.1074/jbc.M200231200.
[11] Broun P, Shanklin J, Whittle E, Somerville C. Catalytic plasticity of fatty acid modification enzymes underlying chemical diversity of plant lipids. Science 1998;282:1315–7. https://doi.org/10.1126/science.282.5392.1315.
[12] Vanhercke T, Shrestha P, Green AG, Singh SP. Mechanistic and structural insights into the regioselectivity of an Acyl-CoA fatty acid desaturase via directed molecular evolution. J Biol Chem 2011;286:12860–9. https://doi.org/10.1074/jbc.M110.191098.
[13] Watanabe K, Ohno M, Taguchi M, Kawamoto S, Ono K, Aki T. Identification of amino acid residues that determine the substrate specificity of mammalian membrane-bound front-end fatty acid desaturases. J Lipid Res 2016;57:89–99. https://doi.org/10.1194/jlr.M064121.
[14] Ding B, Liénard MA, Wang H, Zhao C, Löfstedt C. Terminal fatty-acyl-CoA desaturase involved in sex pheromone biosynthesis in the winter moth (*Operophtera brumata*). Insect Biochem Mol Biol 2011;41:715–22. https://doi.org/10.1016/j.ibmb.2011.05.003.
[15] Cai Y, Yu X-H, Liu Q, Liu C-J, Shanklin J. Two clusters of residues contribute to the activity and substrate specificity of Fm1, a bifunctional oleate and linoleate desaturase of fungal origin. J Biol Chem 2018. jbc.RA118.005972. 10.1074/jbc.RA118.005972.
[16] Ding B-J, Carraher C, Löfstedt C. Sequence variation determining stereochemistry of a Δ11 desaturase active in moth sex pheromone biosynthesis. Insect Biochem Mol Biol 2016;74:68–75. https://doi.org/10.1016/j.ibmb.2016.05.002.
[17] Buček A, Matoušková P, Vogel H, Šebesta P, Jahn U, Weißflog J, et al. Evolution of moth sex pheromone composition by a single amino acid substitution in a fatty acid desaturase. Proc Natl Acad Sci 2015;112:12586–91. https://doi.org/10.1073/pnas.1514566112.
[18] Libisch B, Michaelson LV, Lewis MJ, Shewry PR, Napier JA. Chimeras of Δ6-fatty acid and Δ8-sphingolipid desaturases. Biochem Biophys Res Commun 2000;279:779–85.
[19] Hoffmann M, Hornung E, Busch S, Kassner N, Ternes P, Braus GH, et al. A small membrane-peripheral region close to the active center determines regioselectivity of membrane-bound fatty acid desaturases from *Aspergillus nidulans*. J Biol Chem 2007;282:26666–74. https://doi.org/10.1074/jbc.M705068200.
[20] Hongsthong A, Subudhi S, Sirijuntarat M, Cheevadhanarak S. Mutation study of conserved amino acid residues of Spirulina delta 6-acyl-lipid desaturase showing involvement of histidine 313 in the regioselectivity of the enzyme. Appl Microbiol Biotechnol 2004;66:74–84. https://doi.org/10.1007/s00253-004-1655-x.
[21] Land H, Humble MS. YASARA: A Tool to Obtain Structural Guidance in Biocatalytic Investigations. In: Bornscheuer UT, Höhne M, editors. Protein Eng. Methods Protoc.. Springer; 2018. p. 43–67. https://doi.org/10.1007/978-1-4939-7366-8_4.
[22] Xiang Z. Advances in homology protein structure modeling. Curr Protein Pept Sci 2006;7:217–27.
[23] Holz C, Hesse O, Bolotina N, Stahl U, Lang C. A micro-scale process for high-throughput expression of cDNAs in the yeast *Saccharomyces cerevisiae*. Protein Expr Purif 2002;25:372–8.
[24] Moto K, Suzuki MG, Hull JJ, Kurata R, Takahashi S, Yamamoto M, et al. Involvement of a bifunctional fatty-acyl desaturase in the biosynthesis of the silkmoth, *Bombyx mori*, sex pheromone. Proc Natl Acad Sci U S A 2004;101:8631–6. https://doi.org/10.1073/pnas.0402056101.
[25] Schneiter R, Tatzer V, Gogg G, Leitner E, Kohlwein SD. Elo1p-dependent carboxy-terminal elongation of C14:1Delta(9) to C16:1Delta(11) fatty acids in *Saccharomyces cerevisiae*. J Bacteriol 2000;182:3655–60.
[26] Buček A, Matoušková P, Sychrová H, Pichová I, Hrušková-Heidingsfeldová O. Δ12-Fatty acid desaturase from *Candida parapsilosis* is a multifunctional desaturase producing a range of polyunsaturated and hydroxylated fatty acids. PLoS ONE 2014;9:. https://doi.org/10.1371/journal.pone.0093322e93322.
[27] Buček A, Vogel H, Matoušková P, Prchalová D, Žáček P, Vrkoslav V, et al. The role of desaturases in the biosynthesis of marking pheromones in bumblebee males. Insect Biochem Mol Biol 2013;43:724–31. https://doi.org/10.1016/j.ibmb.2013.05.003.
[28] Rath A, Glibowicka M, Nadeau VG, Chen G, Deber CM. Detergent binding explains anomalous SDS-PAGE migration of membrane proteins. Proc Natl Acad Sci 2009;106:1760–5. https://doi.org/10.1073/pnas.0813167106.
[29] Matoušková P, Pichová I, Svatoš A. Functional characterization of a desaturase from the tobacco hornworm moth (*Manduca sexta*) with bifunctional Z11- and 10,12-desaturase activity. Insect Biochem Mol Biol 2007;37:601–10. https://doi.org/10.1016/j.ibmb.2007.03.004.
[30] Mendiburu F. agricolae 2019. https://www.rdocumentation.org/packages/agricolae.
[31] Edgar RC. MUSCLE: multiple sequence alignment with high accuracy and high throughput. Nucleic Acids Res 2004;32:1792–7. https://doi.org/10.1093/nar/gkh340.
[32] Clamp M, Cuff J, Searle SM, Barton GJ. The Jalview Java alignment editor. Bioinformatics 2004;20:426–7. https://doi.org/10.1093/bioinformatics/btg430.
[33] Hornak V, Abel R, Okur A, Strockbine B, Roitberg A, Simmerling C. Comparison of multiple Amber force fields and development of improved protein backbone parameters. Proteins Struct Funct Bioinforma 2006;65:712–25. https://doi.org/10.1002/prot.21123.
[34] Jämbeck JPM, Lyubartsev AP. An Extension and Further Validation of an All-Atomistic Force Field for Biological Membranes. J Chem Theory Comput 2012;8:2938–48. https://doi.org/10.1021/ct300342n.

[35] Jämbeck JPM, Lyubartsev AP. Another Piece of the Membrane Puzzle: Extending Slipids Further. J Chem Theory Comput 2013;9:774–84. https://doi.org/10.1021/ct300777p.
[36] Jämbeck JPM, Lyubartsev AP. Derivation and Systematic Validation of a Refined All-Atom Force Field for Phosphatidylcholine Lipids. J Phys Chem B 2012;116:3164–79. https://doi.org/10.1021/jp212503e.
[37] Singh UC, Kollman PA. An approach to computing electrostatic charges for molecules. J Comput Chem 1984;5:129–45. https://doi.org/10.1002/jcc.540050204.
[38] Jorgensen WL, Chandrasekhar J, Madura JD, Impey RW, Klein ML. Comparison of simple potential functions for simulating liquid water. J Chem Phys 1983;79:926–35. https://doi.org/10.1063/1.445869.
[39] Essmann U, Perera L, Berkowitz ML, Darden T, Lee H, Pedersen LG. A smooth particle mesh Ewald method. J Chem Phys 1995;103:8577–93. https://doi.org/10.1063/1.470117.
[40] Parrinello M, Rahman A. Polymorphic transitions in single crystals: A new molecular dynamics method. J Appl Phys 1981;52:7182–90. https://doi.org/10.1063/1.328693.
[41] Nosé S. A molecular dynamics method for simulations in the canonical ensemble. Mol Phys 1984;52:255–68. https://doi.org/10.1080/00268978400101201.
[42] Hess B, Bekker H, Berendsen HJC, Fraaije JGEM. LINCS: A linear constraint solver for molecular simulations. J Comput Chem 1997;18:1463–72. https://doi.org/10.1002/(SICI)1096-987X(199709)18:12<1463::AID-JCC4>3.0.CO;2-H.
[43] Miyamoto S, Kollman PA. Settle: An analytical version of the SHAKE and RATTLE algorithm for rigid water models. J Comput Chem 1992;13:952–62. https://doi.org/10.1002/jcc.540130805.
[44] Hess B, Kutzner C, van der Spoel D, Lindahl E. GROMACS 4: Algorithms for Highly Efficient, Load-Balanced, and Scalable Molecular Simulation. J Chem Theory Comput 2008;4:435–47. https://doi.org/10.1021/ct700301q.
[45] Liu W, Jiao H, O'Connor M, Roelofs WL. Moth desaturase characterized that produces both Z and E isomers of delta 11-tetradecenoic acids. Insect Biochem Mol Biol 2002;32:1489–95.
[46] Liu W, Jiao H, Murray NC, O'Connor M, Roelofs WL. Gene characterized for membrane desaturase that produces (E)-11 isomers of mono- and diunsaturated fatty acids. Proc Natl Acad Sci U S A 2002;99:620–4. https://doi.org/10.1073/pnas.221601498.
[47] Hao G, Liu W, O'Connor M, Roelofs WL. Acyl-CoA Z9-and Z10-desaturase genes from a New Zealand leafroller moth species. *Planotortrix octo*. Insect Biochem Mol Biol 2002;32:961–6.
[48] Hao G, O'Connor M, Liu W, Roelofs WL. Characterization of Z/E11- and Z9-desaturases from the obliquebanded leafroller moth. *Choristoneura rosaceana*. J Insect Sci 2002;2:26.
[49] Liu W, Rooney AP, Xue B, Roelofs WL. Desaturases from the spotted fireworm moth (*Choristoneura parallela*) shed light on the evolutionary origins of novel moth sex pheromone desaturases. Gene 2004;342:303–11. https://doi.org/10.1016/j.gene.2004.08.017.
[50] Harpaz Y, Gerstein M, Chothia C. Volume changes on protein folding. Structure 1994;2:641–9. https://doi.org/10.1016/S0969-2126(00)00065-4.
[51] Rodríguez S, Clapés P, Camps F, Fabriàs G. Stereospecificity of an Enzymatic Monoene 1,4-Dehydrogenation Reaction: Conversion of (Z)-11-Tetradecenoic Acid into (E, E)-10,12-Tetradecadienoic Acid. J Org Chem 2002;67:2228–33. https://doi.org/10.1021/jo0109927.